Supplemental Information: Cloning of Quantum Entanglement

Li-Chao Peng,[1,2,*] Dian Wu,[1,2,*] Han-Sen Zhong,[1,2] Yi-Han Luo,[1,2] Yuan Li,[1,2] Yi Hu,[1,2] Xiao Jiang,[1,2] Ming-Cheng Chen,[1,2] Li Li,[1,2] Nai-Le Liu,[1,2] Kae Nemoto,[3] William J. Munro,[4,3] Barry C. Sanders,[1,2,5,6] Chao-Yang Lu,[1,2] and Jian-Wei Pan[1,2]

[1]*Hefei National Laboratory for Physical Sciences at Microscale and Department of Modern Physics, University of Science and Technology of China, Hefei, Anhui 230026, China*
[2]*CAS Center for Excellence and Synergetic Innovation Center in Quantum Information and Quantum Physics, University of Science and Technology of China, Hefei, Anhui 230026, China*
[3]*National Institute of Informatics, 2-1-2 Hitotsubashi, Chiyoda-ku, Tokyo 101-8430, Japan*
[4]*NTT Basic Research Laboratories & NTT Research Center for Theoretical Quantum Physics, NTT Corporation, 3-1 Morinosato-Wakamiya, Atsugi, Kanagawa 243-0198, Japan*
[5]*Institute for Quantum Science and Technology, University of Calgary, Alberta T2N 1N4, Canada*
[6]*Program in Quantum Information Science, Canadian Institute for Advanced Research, Toronto, Ontario M5G 1Z8, Canada*

THE MODEL FOR QUANTUM CLONING OF ENTANGLEMENT

In this section we derive the generalized bipartite entanglement cloning protocol. Without loss of generality, Charlie prepares the initial bipartite pure entangled state $|\phi\rangle_{12} = \alpha\,|01\rangle_{12} + \beta\,|10\rangle_{12}$ with α and β complex coefficients satisfying the normalization condition $|\alpha|^2 + |\beta|^2 = 1$. Then Charles exploits two 1-to-2 single-qubit optimal quantum cloning machines (QCMs) [1], employing partial teleportation [2], to perform bilateral universal quantum cloning. As shown in Fig. 1 of the main text, the quantum state of the initial system including the to-be-cloned state and the two QCMs is

$$\begin{aligned}|\xi\rangle_{\text{initial}} =& |\phi\rangle_{12}\otimes|\Psi^-\rangle_{34}\otimes|\Psi^-\rangle_{56}\\ =&\alpha|0\rangle_1|1\rangle_2\otimes\frac{1}{\sqrt{2}}(|01\rangle-|10\rangle)_{34}\otimes\frac{1}{\sqrt{2}}(|01\rangle-|10\rangle)_{56}+\beta|1\rangle_1|0\rangle_2\otimes\frac{1}{\sqrt{2}}(|01\rangle-|10\rangle)_{34}\otimes\frac{1}{\sqrt{2}}(|01\rangle-|10\rangle)_{56}.\end{aligned} \tag{1}$$

Next proceeding with the $\hat{\boldsymbol{U}}_i$ $(i = 1, 2)$ operations, which are related to the transformations of photons in different modes represented as

$$\begin{cases}\hat{a}_1^\dagger \to i\sqrt{R}\hat{a}_{3'}^\dagger + \sqrt{1-R}\hat{a}_{1'}^\dagger,\\ \hat{a}_3^\dagger \to i\sqrt{R}\hat{a}_{1'}^\dagger + \sqrt{1-R}\hat{a}_{3'}^\dagger,\\ \hat{a}_2^\dagger \to i\sqrt{R}\hat{a}_{5'}^\dagger + \sqrt{1-R}\hat{a}_{2'}^\dagger,\\ \hat{a}_5^\dagger \to i\sqrt{R}\hat{a}_{2'}^\dagger + \sqrt{1-R}\hat{a}_{5'}^\dagger\end{cases}, \tag{2}$$

we postselect with an overall probability of $4/9$ for the events corresponding to each mode having just one and only one photon. Given this, the final six-photon state is

$$\begin{aligned}|\xi\rangle_{\text{final}} =&\frac{\alpha}{2}\big[-(1-2R)R\,|001101\rangle_{1'2'3'45'6}-(1-2R)^2|011001\rangle_{1'2'3'45'6}+(1-2R)(1-R)|011100\rangle_{1'2'3'45'6}\\ &-R^2\,|100101\rangle_{1'2'3'45'6}+(2R-1)R|110001\rangle_{1'2'3'45'6}+(1-R)R\,|110100\rangle_{1'2'3'45'6}\\ &+(1-R)R\,|000111\rangle_{1'2'3'45'6}+(1-R)(1-2R)|010011\rangle_{1'2'3'45'6}-(1-R)^2\,|010110\rangle_{1'2'3'45'6}\big]\\ &+\frac{\beta}{2}\big[-(1-2R)R|110010\rangle_{1'2'3'45'6}-(1-2R)^2|100110\rangle_{1'2'3'45'6}+(1-2R)(1-R)|100011\rangle_{1'2'3'45'6}\\ &-R^2\,|011010\rangle_{1'2'3'45'6}+(2R-1)R\,|001110\rangle_{1'2'3'45'6}+(1-R)R|001011\rangle_{1'2'3'45'6}\\ &+(1-R)R\,|111000\rangle_{1'2'3'45'6}+(1-R)(1-2R)|101100\rangle_{1'2'3'45'6}-(1-R)^2|101001\rangle_{1'2'3'45'6}\big].\end{aligned} \tag{3}$$

From this state of the whole physical system, we obtain the two-photon states of pairs $(1', 2')$ and $(4, 6)$ by tracing over other subsystems in succession.

Now let us rewrite the initial bipartite to-be-cloned state as

$$\rho_{12} = |\phi\rangle_{12}\langle\phi| = \alpha\alpha^*|01\rangle_{12}\langle 01| + \alpha\beta^*|01\rangle_{12}\langle 10| + \beta\alpha^*|10\rangle_{12}\langle 01| + \beta\beta^*|10\rangle_{12}\langle 10|\,. \tag{4}$$

from what the $F := \text{Tr}[\rho\,|\phi\rangle_{12}\langle\phi|]$ can be used as a figure of merit for our cloned states. To illustrate it behaviour we plot the

fidelities of $\rho_{1'2'}$ and ρ_{46} in the top panel of Fig. S1 as a functions of α and R. Here the blue-and-orange mesh surfaces are plotted for $\rho_{1'2'}$ and for ρ_{46}, respectively. We can go further and explore the entanglement properties of photon pairs $(1', 2')$ and $(4, 6)$. To achieve this we construct an entanglement witness operator $\hat{\boldsymbol{W}}$, which has negative expectation value $\mathrm{Tr}[\hat{\boldsymbol{W}}\rho] < 0$ for an entangled state ρ. The expectation value $\langle\hat{\boldsymbol{W}}(\alpha, R)\rangle$ (ranging from -0.5 to 0.25) is illustrated in the bottom panel of Fig. S1. The blue surface represents $\rho_{1'2'}$ and the orange surface represents ρ_{46}, while the green surface is the boundary $\langle\hat{\boldsymbol{W}}(\alpha, R)\rangle = 0$. Clearly, there is a close space surrounded by these three surfaces with negative $\langle\hat{\boldsymbol{W}}(\alpha, R)\rangle$, which indicates that both ρ_{46} and $\rho_{1'2'}$ are genuine entangled states under the corresponding conditions of parameters α and R.

Further in the case where the initial state $|\phi\rangle_{12}$ is a maximally entangled state expressed as $|\Psi^+\rangle = \frac{1}{\sqrt{2}}(|01\rangle + |10\rangle)$, the quantum states of photon pairs $(1', 2')$ and $(4, 6)$ at the end of the protocol are

$$\begin{aligned}
\rho_{1'2'} =&[\frac{1}{4}(1-2R)^2R^2 + \frac{1}{4}(1-R)^2R^2]\,|00\rangle\langle 00| \\
&+[\frac{1}{4}(1-2R)^2(1-R)^2 + \frac{1}{8}(1-R)^4 + \frac{1}{8}(1-2R)^4 + \frac{1}{8}R^4]\,|01\rangle\langle 01| \\
&+[\frac{1}{4}(1-2R)^2(1-R)^2 + \frac{1}{8}(1-R)^4 + \frac{1}{8}(1-2R)^4 + \frac{1}{8}R^4]\,|10\rangle\langle 10| \\
&+[\frac{1}{2}(1-2R)^2(1-R)^2]\,|01\rangle\langle 10| + [\frac{1}{2}(1-2R)^2(1-R)^2]|10\rangle\langle 01| \\
&+[\frac{1}{4}(1-2R)^2R^2 + \frac{1}{4}(1-R)^2R^2]\,|11\rangle\langle 11|. \\
\rho_{46} =&[\frac{1}{4}(1-2R)^2R^2 + \frac{1}{4}(1-2R)^2(1-R)^2]\,|00\rangle\langle 00| \\
&+[\frac{1}{4}(1-R)^2R^2 + \frac{1}{8}(1-R)^4 + \frac{1}{8}R^4 + \frac{1}{8}(1-2R)^4]\,|01\rangle\langle 01| \\
&+[\frac{1}{4}(1-R)^2R^2 + \frac{1}{8}(1-R)^4 + \frac{1}{8}R^4 + \frac{1}{8}(1-2R)^4]\,|10\rangle\langle 10| \\
&+[\frac{1}{2}(1-R)^2R^2]\,|01\rangle\langle 10| + [\frac{1}{2}(1-R)^2R^2]\,|10\rangle\langle 01| \\
&+[\frac{1}{4}(1-2R)^2R^2 + \frac{1}{4}(1-2R)^2(1-R)^2]\,|11\rangle\langle 11|.
\end{aligned} \tag{5}$$

It is straight forward now to show the corresponding fidelities are

$$\begin{aligned}
F_{1'2'} =& \frac{2(1-2R)^2(1-R)^2 + (2 - 12R + 28R^2 - 30R^3 + 13R^4)}{4(3R^2 - 3R + 1)^2} \\
F_{46} =& \frac{2R^2(1-R)^2 + (1 - 6R + 16R^2 - 20R^3 + 10R^4)}{4(3R^2 - 3R + 1)^2}.
\end{aligned} \tag{6}$$

In Fig. S2 a we plot the fidelities of pairs $(1', 2')$ and $(4, 6)$ as a function of R. Immediately we observe that there is a small range of R from 0.304 to 0.360 where both $\rho_{1'2'}$ and ρ_{46} show entanglement properties. In particular, at $R = 1/3$, the QCMs produce two identical entangled copies with $F_{1'2'} = F_{46} = 7/12$. This was the initial reason for the choice of R shown in the main text.

It is useful to explore this $R = 1/3$ case a little more. If we return to our more general initial bipartite state of the form $|\phi\rangle_{12} = \alpha\,|01\rangle_{12} + \beta\,|10\rangle_{12}$ then it is straightforward to determine the fidelity $F_\phi = \mathrm{Tr}[\sigma\,|\phi\rangle_{12}\langle\phi|]$ as well as $F_{\Psi^+} = \mathrm{Tr}[\sigma|\Psi^+\rangle\langle\Psi^+|]$ where $\sigma = \rho_{1'2'} = \rho_{46}$. We plot those fidelities in Fig. S2 b and immediately observe that $\alpha = 1/\sqrt{2}$ gives the lowest value of the cloning fidelity, however those output copies are entangled with $F_{\Psi^+} > 0.5$ for an $\alpha \in [0.332, 0.943]$ range. This clearly shows our protocol enables entanglement broadcasting for a wide range of states with both the output copies in inseparable states.

Further we can also determine important properties of the quantum states of other pairs $(1', 6)$, $(1', 4)$, $(2', 6)$ and $(2', 4)$. Interestingly, due to the symmetric distribution of information in our single qubit cloning machines with $R = 1/3$, $F_{1'2'} = F_{46} = F_{1'6} = F_{2'4}$, while $F_{1'4} = F_{2'6}$. This in turns means that with $|\Psi^+\rangle_{12} = \frac{1}{\sqrt{2}}(|01\rangle_{12} + |10\rangle_{12})$ as our state to be cloned, our resulting state fidelities are $F_{1'2'} = F_{46} = F_{1'6} = F_{2'4} = 7/12$ with $F_{1'4} = F_{2'6} = 1/3$. These are shown in Fig. S2 c. We can also determine the degree of entanglement and mixture by calculating the concurrence [3] and von Neumann entropy [4]. The concurrence is defined as $C(\rho) =: \max\{0, \lambda_1 - \lambda_2 - \lambda_3 - \lambda_4\}$, where λ_i are the eigenvalues of the Hermitian matrix $R = \sqrt{\sqrt{\rho}\widetilde{\rho}\sqrt{\rho}}$ arranged in decreasing order, with $\widetilde{\rho} = (\sigma_y \otimes \sigma_y)\rho^*(\sigma_y \otimes \sigma_y)$ being the spin-flipped state of ρ. The von Neumann entropy is calculated by $S(\rho) =: -\Sigma_i p_i \log[p_i]$ with p_i the eigenvalues of ρ. For our situation here with $R = 1/3$ we

obtain $C(\rho_{1'2'}) = C(\rho_{46}) = \frac{1}{6} \approx 0.167$ and $S(\rho_{1'2'}) = S(\rho_{46}) \approx 1.137$ (The concurrence ranges from 0 for separable states to 1 for maximally entangled states while the von Neumann entropy ranges from 0 for pure states to $\log[d]$ (d is the state space dimension) for fully mixed states). This clearly shows the entanglement in both the local and distant cloned states.

ANALYSIS OF EXPERIMENTAL IMPERFECTION

In this section, we analyze various imperfections and error sources in our experiments. These imperfections and error sources are then taken into account in our modeling the state fidelities of the output states.

Double-pair emission in SPDC source. In multi-photon experiments using SPDC sources, one of the main causes of experimental noise is double-pair emission due to the probabilistic nature of photon pair generation in SPDC [5]. In our experiment, we employ a three entangled-photon pair source using SPDC. Without loss of generality, the state generated from each source can be described as

$$|\psi\rangle \sim |\text{vac}\rangle + \sqrt{\frac{p}{2}}\left(\hat{a}_H^\dagger \hat{b}_V^\dagger - \hat{a}_V^\dagger \hat{b}_H^\dagger\right)|\text{vac}\rangle + \frac{p}{2}\left(\frac{\hat{a}_H^\dagger \hat{b}_V^\dagger - \hat{a}_V^\dagger \hat{b}_H^\dagger}{\sqrt{2}}\right)^2 |\text{vac}\rangle\,. \tag{7}$$

where $\hat{a}^\dagger$ and $\hat{b}^\dagger$ are the creation operators of the spatial modes a and b with H and V denoting the horizontal and vertical polarization, respectively. Further p is the single-pair emission probability. The vacuum state is expressed as $|\text{vac}\rangle$. Third and higher-order terms are improbable and so ignored here.

The effect of double-pair emission is that it can lead to undesirable six-photon coincidences, which manifests as noise in our experiment. To suppress this effect, our experiment works with low laser power so that the single-pair-generation probability per single pulse p is less than 0.01. Thus, the double-pair emission probability is two orders of magnitude smaller than the single-pair emission probability. In our experiment, we do post-selections by selecting the cases where only one photon is recorded in each modes, which make the only way to collect a 6-fold coincidence is if source 1, 2 and 3 emit photon pair (probability $\sim p^3$). The double-pair from any of these sources is then an event with probability of $\sim p^4$ and quite unlikely. For these reasons, here we can safely neglect this effect.

The partial Bell-state measurement. One of the essential steps in our experiment is the operation of our partial Bell-state measurement on the asymmetrical non-polarizing beam splitters with reflectivity $R = 1/3$. In theory, the transformation due to a lossless beam splitter for a single photon are

$$\begin{aligned}
\hat{a}_H^\dagger &\to t_H \cdot \hat{a}_H^\dagger + e^{i\delta_{R,H}} r_H \cdot \hat{b}_H^\dagger \\
\hat{b}_H^\dagger &\to t_H \cdot \hat{b}_H^\dagger - e^{-i\delta_{R,H}} r_H \cdot \hat{a}_H^\dagger \\
\hat{a}_V^\dagger &\to e^{i\delta_{T,V}} t_V \cdot \hat{a}_V^\dagger + e^{i\delta_{R,V}} r_V \cdot \hat{b}_V^\dagger \\
\hat{b}_V^\dagger &\to e^{-i\delta_{T,V}} t_V \cdot \hat{b}_V^\dagger - e^{-i\delta_{R,V}} r_V \cdot \hat{a}_V^\dagger
\end{aligned} \tag{8}$$

where t_H (r_V) denotes the amplitude coefficient of the transmission (reflectivity) component for the horizontal (vertical) polarized photons. The creation operators $a^\dagger$ and $b^\dagger$ correspond to the two modes of the beam splitter.

Under ideal conditions, we expect that $t_H^2 = t_V^2 = t^2 = 2/3$ and $r_H^2 = r_V^2 = r^2 = 1/3$ with the phase-shift between the H- and V-polarized photons being equal in each output mode we expect a HOM-type interference visibility of 0.8. Here the visibility is defined as $V := (C_{\text{max}} - C_{\text{min}})/C_{\text{max}} = 1 - (\frac{(1-2r^2)^2}{(1-r^2)^2+r^4})$ where C_{max} and C_{min} are the maximum and minimum four-fold coincidences, respectively. However, real beam splitters are never perfect in terms of their splitting ratio and phase. In our experiment, thanks to the high-precision polarization-independent optical coating, we obtain near-optimal splitting ratios with small fluctuations. Also, by using a combination of two quarter-wave plates and one half-wave plate in each input mode, we are able to control the additional phase introduced by the NBSs.

Indistinguishability between photons. In our experiments, we superpose the photons from two independent SPDC sources on non-polarizing beam splitters (NBSs) and collect six-fold coincidences. A simplified experimental layout is shown in Fig. S3 a. While the photons could be distinguishable in polarization, frequency, time and other degree of freedom, for simplicity, we model these effects with spatio-temporal mode-mismatch. As a simple example shown in Fig. S3 b, the effect of mode-mismatch is written as $a_{H(V)} \to \sqrt{k}\, a_{H(V)} + \sqrt{1-k}\, a_{H'(V')}$ with a mismatch coefficient k. Therein $H(V)$-polarized photons between two input modes can perfectly interfere, however, the H' (V') polarized photons never interfere with H (V) photons.

Now providing that we have prepared H-polarized photon in mode a and b, our state can be expressed as $\hat{a}_H^\dagger \hat{b}_H^\dagger |00\rangle$. The

effect of mode-mismatch leads to a state of the form

$$\begin{aligned}&(\frac{\sqrt{2}}{3}i\sqrt{k}\hat{a}_H^2-\frac{1}{3}\sqrt{1-k}\hat{a}_H\hat{b}_{H'}+\frac{1}{3}\sqrt{k}\hat{a}_H\hat{b}_H+\frac{\sqrt{2}}{3}i\sqrt{k}\hat{b}_H^2\\&+\frac{2}{3}\sqrt{1-k}\hat{a}_{H'}\hat{b}_H+\frac{\sqrt{2}}{3}i\sqrt{1-k}\hat{b}_H\hat{b}_{H'}+\frac{\sqrt{2}}{3}i\sqrt{1-k}\hat{a}_H\hat{a}_{H'})^\dagger\left|00\right\rangle.\end{aligned}\tag{9}$$

where the probability that we record one photon in each output mode is

$$p_{\text{coin}}=\frac{\left(\frac{1}{3}\sqrt{k}\right)^2+\left(\frac{2}{3}\sqrt{1-k}\right)^2+\left(\frac{1}{3}\sqrt{1-k}\right)^2}{2\left(\frac{1}{3}\times2\sqrt{k}\right)^2+\left(\frac{1}{3}\sqrt{1-k}\right)^2+\left(\frac{1}{3}\sqrt{k}\right)^2+\left(\frac{2}{3}\sqrt{1-k}\right)^2+\left(\frac{\sqrt{2}}{3}\sqrt{1-k}\right)^2+\left(\frac{\sqrt{2}}{3}\sqrt{1-k}\right)^2}=\frac{5-4k}{9}.\tag{10}$$

In the scenario that the photons in mode a are fully mismatched ($k=0$), the coincidence probability $5/9$ leading to the visibility of four-fold coincidences as

$$V(k)=\left(\frac{5}{9}-p_{\text{coin}}\right)/\frac{5}{9}=\frac{4k}{5}.\tag{11}$$

As shown in Fig. S4, we have measured our four-fold coincidence rate and obtain a raw visibility of 0.731 ± 0.007. To estimate the value of fraction k, a further step is performed to subtract the background of accidental four-fold coincidences. To illuminate this point further let us consider a pulsed laser with repetition of $\mathcal{R}$ simultaneously pumping two SPDC entangled sources termed ab and cd with photons in modes b and c guided for interference on a NBS. Four kinds of two-fold coincidences can be detected: $\tilde{C}_{a-b}$, $\tilde{C}_{a-c}$, $\tilde{C}_{b-d}$ and $\tilde{C}_{c-d}$. The detected four-fold coincidences per second could be $\tilde{C}_{\text{four-fold}}=(\tilde{C}_{a-b}\tilde{C}_{c-d}+\tilde{C}_{a-c}\tilde{C}_{b-d})/\mathcal{R}$, where $\tilde{C}_{\square}$ is the measured coincidence which includes the real coincidence $C_{\square}$ and the accidental coincidence $A_{\square}$. For example, the detected two-fold coincidences $\tilde{C}_{a-b}$ is equal to $C_{a-b}+A_{a-b}=C_{a-b}+S_aS_b/\mathcal{R}$, with S_a and S_b indicating the single counts of detectors a and b, respectively. Therefore, in experiments, the detected four-fold coincidences per second is

$$\tilde{C}_{\text{four-fold}}=\left[\left(C_{a-b}+\frac{S_aS_b}{\mathcal{R}}\right)\left(C_{c-d}+\frac{S_cS_d}{\mathcal{R}}\right)+\left(C_{a-c}+\frac{S_aS_c}{\mathcal{R}}\right)\left(C_{b-d}+\frac{S_bS_d}{\mathcal{R}}\right)\right]/\mathcal{R}=C_{\text{four-fold}}+A_{\text{four-fold}},\tag{12}$$

where $C_{\text{four-fold}}=\left(C_{a-b}C_{c-d}+C_{a-c}C_{b-d}\right)/\mathcal{R}$ and $A_{\text{four-fold}}=(C_{a-b}S_cS_d+C_{c-d}S_aS_b+C_{a-c}S_bS_d+C_{b-d}S_aS_c)/\mathcal{R}^2+2S_aS_bS_cS_d/\mathcal{R}^3$. In this way, we calculate the incidental four-fold counts $A_{\text{four-fold}}$ and then subtract it from the measured four-fold coincidences. Using this method we estimate $k\sim0.932$ in our experiment.

Having estimated the mode-mismatch coefficient we evaluate its impact on the fidelities of our output states when our systems combined input state is

$$\left|\psi\right\rangle_{\text{initial}}=\left|\Phi^+\right\rangle_{12}\left|\Psi^-\right\rangle_{34}\left|\Psi^-\right\rangle_{56}.\tag{13}$$

Consider that the photons in modes 3 and 5 are mismatched with the photons in modes 1 and 2. The transformations of photon in each mode can be expressed as

$$\begin{aligned}\hat{a}_{1H}^\dagger&\to\sqrt{1-R}\hat{a}_{1H}^\dagger+i\sqrt{R}\hat{a}_{3H}^\dagger,\hat{a}_{1V}^\dagger\to\sqrt{1-R}\hat{a}_{1V}^\dagger+i\sqrt{R}\hat{a}_{3V}^\dagger,\\\hat{a}_{2H}^\dagger&\to\sqrt{1-R}\hat{a}_{2H}^\dagger+i\sqrt{R}\hat{a}_{5H}^\dagger,\hat{a}_{2V}^\dagger\to\sqrt{1-R}\hat{a}_{2V}^\dagger+i\sqrt{R}\hat{a}_{5V}^\dagger,\\\hat{a}_{3H}^\dagger&\to\sqrt{k}\left(\sqrt{1-R}\hat{a}_{3H}^\dagger+i\sqrt{R}\hat{a}_{1H}^\dagger\right)+\sqrt{1-k}\left(\sqrt{1-R}\hat{a}_{3H'}^\dagger+i\sqrt{R}\hat{a}_{1H'}^\dagger\right),\\\hat{a}_{3V}^\dagger&\to\sqrt{k}\left(\sqrt{1-R}\hat{a}_{3V}^\dagger+i\sqrt{R}\hat{a}_{1V}^\dagger\right)+\sqrt{1-k}\left(\sqrt{1-R}\hat{a}_{3V'}^\dagger+i\sqrt{R}\hat{a}_{1V'}^\dagger\right),\\\hat{a}_{5H}^\dagger&\to\sqrt{k}\left(\sqrt{1-R}\hat{a}_{5H}^\dagger+i\sqrt{R}\hat{a}_{2H}^\dagger\right)+\sqrt{1-k}\left(\sqrt{1-R}\hat{a}_{5H'}^\dagger+i\sqrt{R}\hat{a}_{2H'}^\dagger\right),\\\hat{a}_{5V}^\dagger&\to\sqrt{k}\left(\sqrt{1-R}\hat{a}_{5V}^\dagger+i\sqrt{R}\hat{a}_{5V}^\dagger\right)+\sqrt{1-k}\left(\sqrt{1-R}\hat{a}_{5V'}^\dagger+i\sqrt{R}\hat{a}_{5V'}^\dagger\right).\end{aligned}\tag{14}$$

By selecting the six-fold coincidence and tracing over the other photons, the state fidelities of photon pairs $(1',2')$ and $(4,6)$

are

$$F_{1'2'} = \frac{0.1163 + R(-0.6821 + R(1.5076 + (-1.4884 + 0.5756R)R))}{0.1163 + R(-0.6821 + R(1.6821 + R(R-2)))},$$
$$F_{46} = \frac{0.0290 + R(-0.1705 + R(0.4963 + (-0.6516 + 0.3258R)R))}{0.1163 + R(-0.6821 + R(1.6821 + R(R-2)))}. \quad (15)$$

which we plot in Fig. S5. Clearly the fidelity of the distant state is more sensitive to the mode-mismatch noise than the fidelity of local state, which implies the experimental challenge for observing entanglement broadcasting due to the small noise-tolerance.

Further our model using realistic parameters is also useful for subtracting the noise from experimental measured fidelities. The aforementioned noise can produce undesired six-fold coincidences which we cannot distinguish. Figure S3 c illustrates these effects by showing that, when several photons in one of the NBS input modes suffers a mode mismatch, three operations that contribute to undesired six-fold coincidences. With the known fraction of mode-mismatch, we are able to subtract this noise.

Next in Fig. S6 we plot the experimental measurement setting for the cloning of a Bell state of the form $(|HV\rangle + |VH\rangle)/\sqrt{2}$. The fidelities calculated by using the raw data are 0.543 ± 0.013 and 0.510 ± 0.013 for the local and distant two-photon states, respectively. Using the correction methods we estimate the corrected state fidelities are 0.526 ± 0.015 and 0.548 ± 0.014 for local and distant two-photon states, respectively. It is important here to mention that the correction methods for local and distant states are different. When the photons do not interfere on one or two NBSs, the distant two-photon state is maximally mixed; thus, we can obtain the modified state by subtracting a maximally-mixed state with a weight. However, these three cases (in Fig. S3 c) have different effects on the fidelity of the local state.

Finally from these measurements, we also carry out an analysis for the quantum states of pairs $(1', 6)$, $(2', 4)$, $(2', 6)$ and $(1', 4)$ to determine their properties. As shown in Fig. S7, quantum entanglement appears in states $\rho_{1'2'}$, ρ_{46}, $\rho_{1'6}$ and $\rho_{2'4}$, while there is no entanglement between pairs $(2', 6)$ and $(1', 4)$, which is in agreement with the theoretical predictions. The fidelities could be improved by reducing the experimental noise, as well as by increasing the data accumulation time meaning the error bar associated with the statistical significance can be minimised. We envision that these challenges can be overcome with increasing precision of quantum operations and long-term stabilisation of our experimental platform.

---

* L.-C. P. and D. W. contributed equally to this work.

[1] Buzek, V. & Hillery, M. Quantum copying: Beyond the no-cloning theorem. *Phys. Rev. A* **54**, 1844 (1996).

[2] Zhao, Z., *et al*. Experimental realization of optimal asymmetric cloning and telecloning via partial teleportation. *Phys. Rev. Lett.* **95**, 030502 (2005).

[3] Wootters, W. K. Entanglement of formation of an arbitrary state of two qubits. *Phys. Rev. Lett.* **80**, 2245 (1998).

[4] Nielsen, M. A. and Chuang, I. L. Quantum Computation and Quantum Information. *Cambridge Univ. Press*, (2000).

[5] Pan, J. W., *et al*. Multiphoton entanglement and interferometry. *Rev. Mod. Phys.* **84**, 777 (2012).

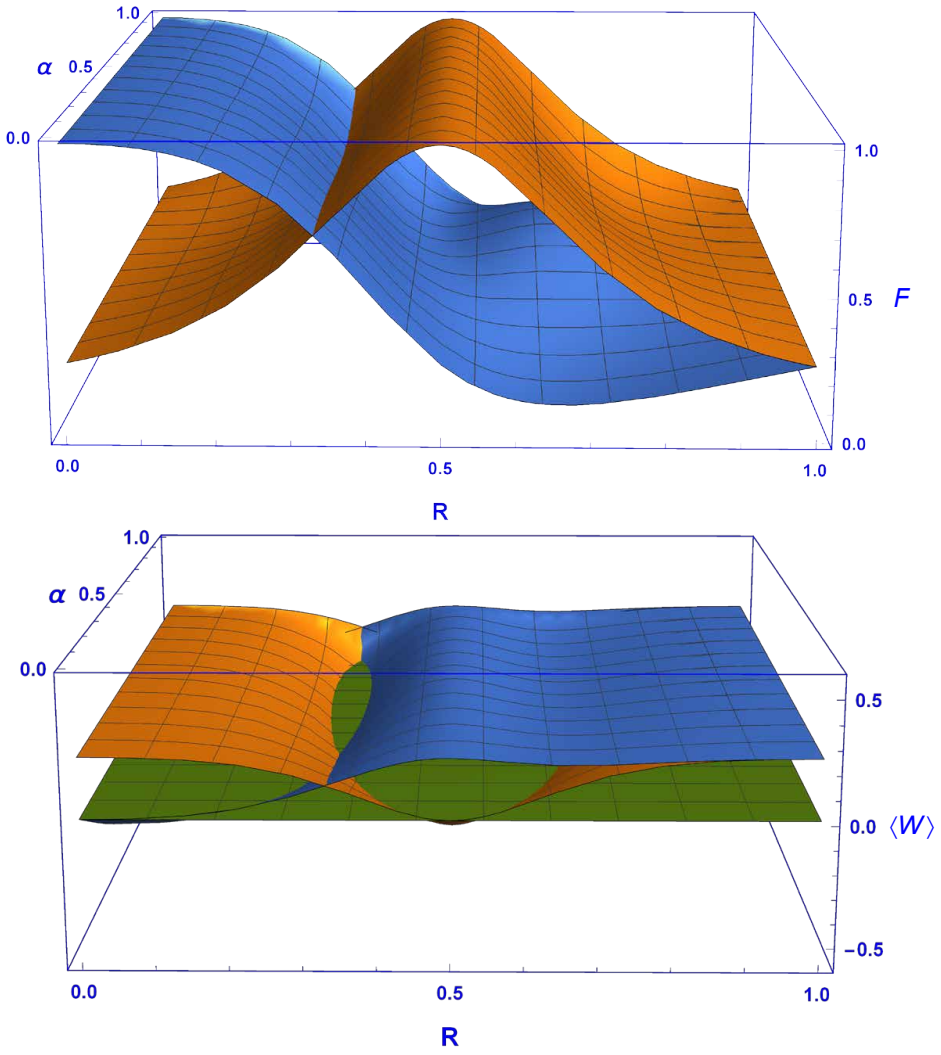

FIG. S1. **Properties of the two output states $\rho_{1'2'}$ and ρ_{46} as a function of the reflectivity R and state parameter α.** The top panel shows the cloning fidelities F with respect to the initial state $|\phi\rangle_{12} = \alpha\,|01\rangle_{12} + \beta\,|10\rangle_{12}$. The bottom panel shows the expectation value of entanglement witness $\langle\hat{\boldsymbol{W}}\rangle$. Here the orange surface is plotted for the distant two-photon state ρ_{46} while the blue surface is for the local two-photon state $\rho_{1'2'}$. In addition the green plane is added marking the $\langle\hat{\boldsymbol{W}}\rangle = 0$ boundary.

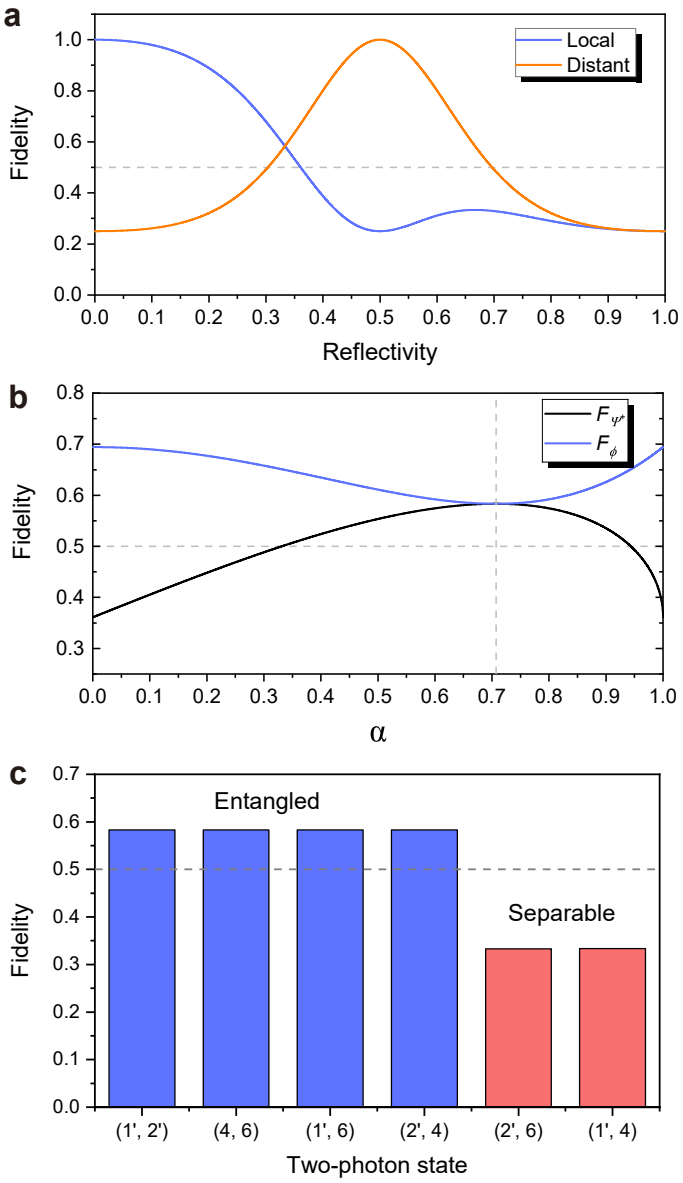

FIG. S2. **Fidelities of the two-photon states $\rho_{1'2'}$ and ρ_{46}. a,** The fidelities vary with R if the initial state is in maximally-entangled states. Here the blue line represents the local two-photon state $\rho_{1'2'}$ while the orange line is for the distant two-photon state ρ_{46}. The gray dashed line is the limit of 0.5. In **b,** we show the fidelities of the two-photon states for various α with $R = 1/3$. The black line corresponds to the overlap with state $|\Psi^+\rangle = \frac{1}{\sqrt{2}}(|01\rangle + |10\rangle)$ while the blue line corresponds to the initial state $|\phi\rangle_{12} = \alpha\,|01\rangle_{12} + \beta\,|10\rangle_{12}$. **c,** depicts the fidelities of the quantum states of two-photon pairs.

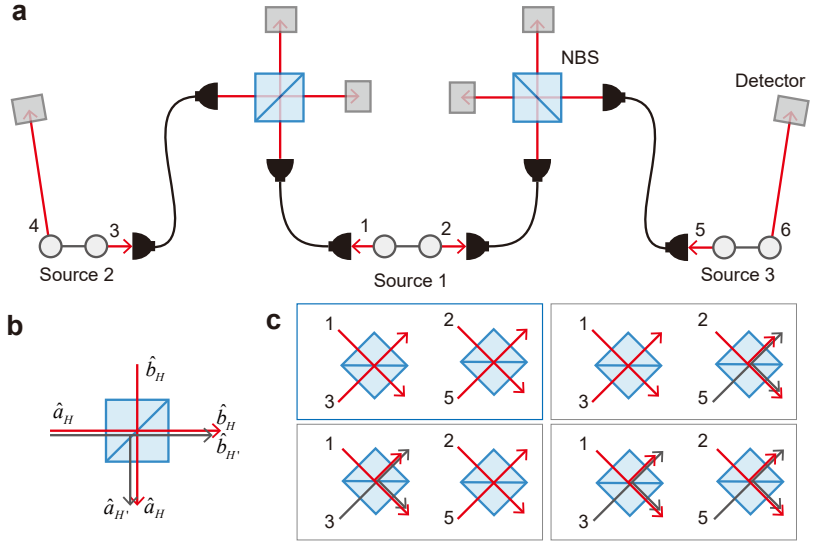

FIG. S3. **The effect of mode-mismatch on interference. a,** A schematic layout of three SPDC sources and interference structures. **b,** Diagram illustrating the effect of mode-mismatch on a BS. **c,** The four operations of the NBSs that produce six-photon events. The red light represents perfect interference while the gray light represents that the photon is in an ancillary mode without quantum interference.

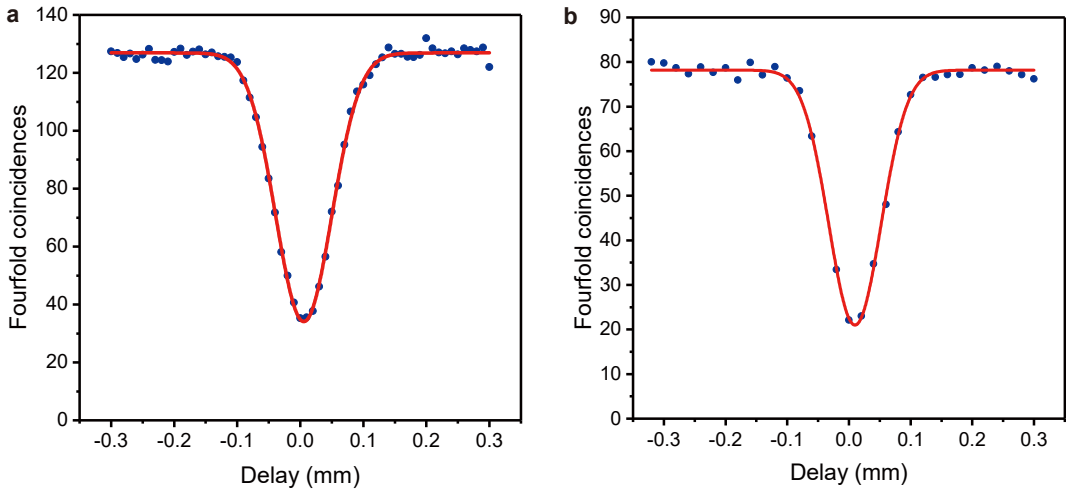

FIG. S4. **Hong-Ou-Mandel type interference between independent SPDC sources. a,** The four-fold coincidences per second with photons from source 1 and source 2. **b,** The four-fold coincidences per second with photons from source 1 and source 3. The red curves are fitted with a Gaussian function.

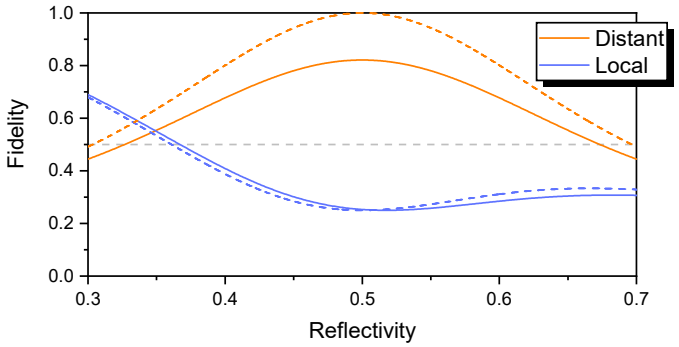

FIG. S5. **Fidelities modelling with mode-mismatch noise.** The dotted lines represent the ideal fidelities of the local and distant cloned states while the solid lines show the expected fidelities using experimental parameters including error estimates. The dashed gray line shows the limit of 0.5.

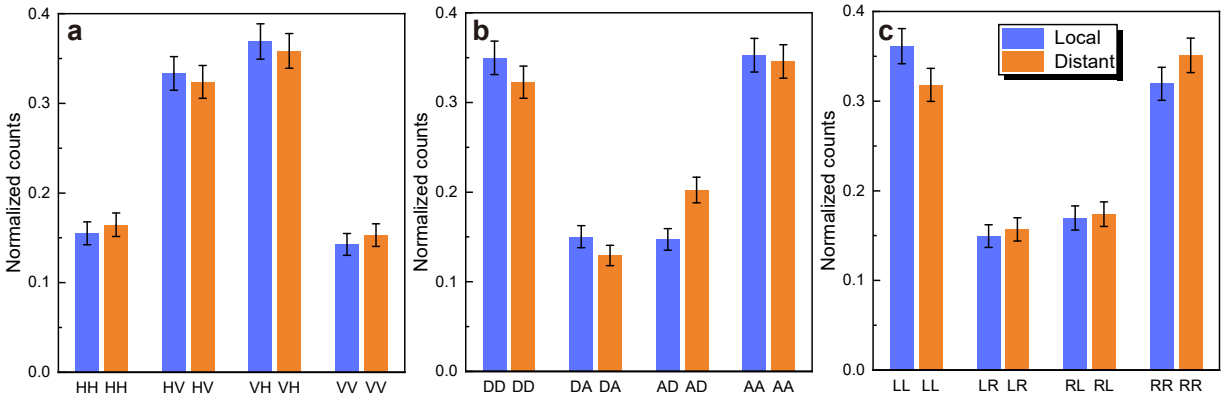

FIG. S6. **Experimental measurement settings for cloning of** $|\phi\rangle_{12} = (|HV\rangle_{12} + |VH\rangle_{12})/\sqrt{2}$**. a,** In the linear basis, the measured expectation values for $\langle\hat{\sigma}_z\hat{\sigma}_z\rangle$ are -0.405 ± 0.030 and -0.365 ± 0.030 respectively for the local and distant cloned states. **b,** In the diagonal basis, the measured expectation values for $\langle\hat{\sigma}_x\hat{\sigma}_x\rangle$ is 0.405 ± 0.029 and 0.337 ± 0.030 respectively. **c,** In the circular basis, the measured expectation values for $\langle\hat{\sigma}_y\hat{\sigma}_y\rangle$ is 0.362 ± 0.030 and 0.338 ± 0.031 for local and distant two-photon states, respectively. Without subtracting the background noise, the fidelities calculated by $F = \frac{1}{4}\,\mathrm{Tr}\left[\tilde{\rho}_{\mathrm{exp}}\left(\hat{\boldsymbol{I}} + \langle\hat{\sigma}_x\hat{\sigma}_x\rangle + \langle\hat{\sigma}_y\hat{\sigma}_y\rangle - \langle\hat{\sigma}_z\hat{\sigma}_z\rangle\right)\right]$ are 0.543 ± 0.013 and 0.510 ± 0.013 respectively. The error bars are one standard deviation calculated with Poissonian counting statistics of raw counts. The accumulation time for each setting is 2 hours.

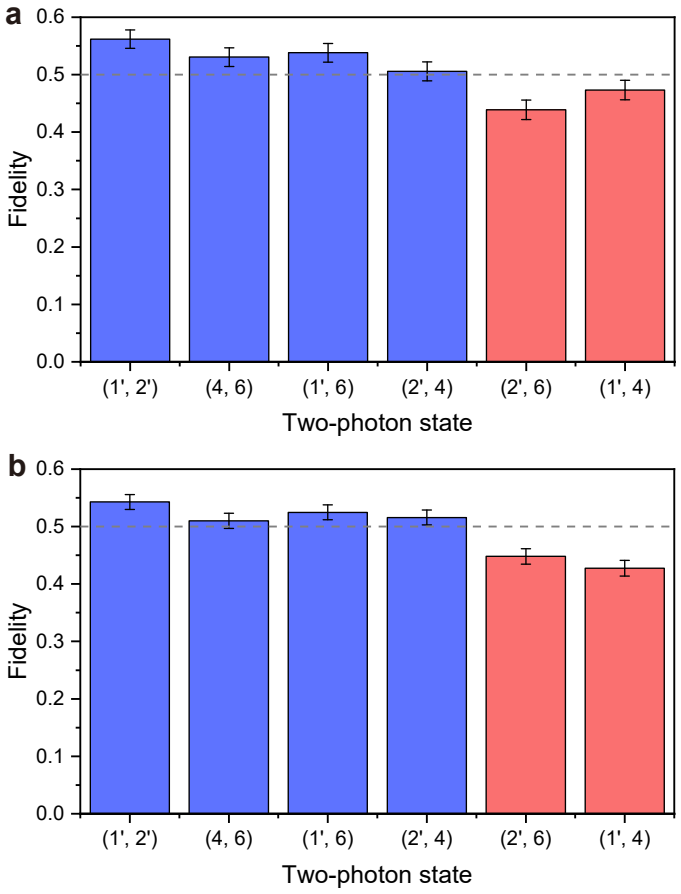

FIG. S7. **Fidelities of the two-photon states with symmetrical cloning operations.** In **a,** the measured fidelities of reduced states for photon pairs $(1', 2')$, $(4, 6)$, $(1', 6)$, $(2', 4)$, $(2', 6)$ and $(1', 4)$ with the initial two-qubit state in $(|HH\rangle_{12} + |VV\rangle_{12})/\sqrt{2}$. Similarly for **b** the measured fidelities are shown for the initial state $(|HV\rangle_{12} + |VH\rangle_{12})/\sqrt{2}$. The error bars are one standard deviation calculated with Poissonian counting statistics of raw counts.